

## Corrosion Behavior of X70 and X80 Pipeline Steels in Simulated Soil Solution

Xinhua Wang, Xuting Song, Yingchun Chen<sup>\*</sup>, Zuquan Wang, Liuwei Zhang

College of Mechanical Engineering and Applied Electronics Technology, Beijing University of Technology, Beijing 100124, China

<sup>\*</sup>E-mail: [ychen08089@163.com](mailto:ychen08089@163.com)

*Received:* 9 March 2018 / *Accepted:* 21 April 2018 / *Published:* 5 June 2018

---

Corrosion behavior of X70 and X80 steel in simulated soil solution with AC interference was studied by applied open circuit potential, polarization curve, scanning electron microscope and gravimetry. The corrosion potential of X70 and X80 steel shifted negatively with increasing AC density. Polarization curves were all in active dissolution zone without passivation area. At the low AC density (0-100 A/m<sup>2</sup>), the corrosion rate of X70 steel increased rapidly with the density increase, while the change of corrosion rate of X70 steel was not as obvious at high AC density (100-300 A/m<sup>2</sup>). Under the AC interference with density of 0–300 A/m<sup>2</sup>, the corrosion rate of X80 steel increased steadily with the increase of AC density. At the same AC density, the corrosion rate of X70 steel was about 2 times higher than that of X80 steel. At the low AC density, the surface morphology of the corroded X70 showed uniform corrosion: the sample surface was relatively smooth. At the high AC density, more numerous and larger corrosion pits were observed. When AC density was 0–200 A/m<sup>2</sup>, the corrosion morphology of X80 steel was uniform with the smooth surface, only with some pitting corrosion at 300 A/m<sup>2</sup> AC density. Thus, corrosion resistance of X80 steel was better than that of X70 steel in simulated soil solutions.

---

**Keywords:** X70 steel, X80 steel, alternating current, corrosion rate

### 1. INTRODUCTION

Energy transport through pipelines has important advantages over other means such as large capacity, low cost and high safety. Because of these, pipeline transportation is rapidly developing around the world. Currently, natural gas pipelines account for 66.3% of the total length of oil and gas pipelines around the world [1]. To save on pipeline construction costs, large-diameter and high-pressure pipelines with the high-strength steel are used in large quantities.

In the 1950s and 1960s, the maximum delivery pressure within the pipeline was 6.3 MPa, while in the 70-80s and then 90s it was 10 MPa, and 14 MPa, respectively. By the 21st century, the operational pressure of gas pipelines reached 15-20 MPa and even higher in some cases. With the continuous increase of pressure in pipeline transportation, pipeline steel requirements as quickly upgraded to high-grade steel with larger diameter to withstand higher pipe pressure. The X52 pipeline steel was used in the 1960s, and the X60 ~ X65 pipeline steel was widely used in the 1970s. Currently, X70 pipeline steel is mostly used, yet, X80 pipeline steel is also starting to be widely utilized.

Because of the recent rapid development of oil and gas industry in China, the advanced pipeline steel is needed [2]. During the second phase of the west-to-east gas transmission project, Chinese government invested 15 billion dollars to use mainly X70 pipeline steel. However, during the pipeline construction, the problem of the pipeline corrosion emerged, which is also inevitable during the actual operation [3-7]. Some researchers analyzed the influencing factors of oil and gas pipeline corrosion, summarized the corrosion mechanisms caused by different factors, and compared the advantages and disadvantages of pipeline protection methods [8-12]. Because of the different chemical composition, the corrosion behavior of different types of pipeline steel is not the same [13]. Corrosion occurs around the boundaries of the alloy grains, while the corrosion of grains themselves is only minor. The accumulation of C, P, S and other inclusions in the boundary of grain leads to lower potential comparing to the grain itself. The metals are more active and prone to corrosion at lower potentials. Therefore C, P and S affect corrosion behavior of the pipeline steel [14] causing different corrosion resistance of various types of steel.

With the rapid construction of high voltage AC transmission line and AC electrified railway, the buried steel pipelines become more vulnerable to the AC interference. This interference is one of the important reasons of the buried pipeline corrosion[15-17]. There are many AC corrosion theories [18-27] such as Faraday rectification [28], irreversibility of anode reaction [29], depolarization of anode reaction [30], oscillation of AC voltage at metal/dielectric interface [31], etc. Goidanich [32] obtained the law of corrosion rate change for carbon steel under different AC densities by gravimetry. Fu and Cheng [33] studied the influence of AC on passivation behavior of X65 steel in a carbonate environment. Jiang shed light on the effect of AC density and frequency on the corrosion potential of Q235 steel. Weng found that corrosion rate of Q235 steel and AC interference intensity comply with the law of power function. Xu [34] researched and developed a real-time AC/DC data acquisition device. Ormellese [35] investigated the change of the local corrosion resistance of stainless steel and how it is affected by the different chemical compositions of the simulated soil solutions at various AC densities and concluded that the influence of AC stray can be evaluated by corrosion time, critical AC density and corrosion morphology. Li [36] also conducted an experimental study on the corrosion behavior of X70 pipeline steel exposed to AC under the marine conditions and suggested that the corrosion rate of X70 pipeline increased with AC density increase.

Corrosion behavior of X80 steel under AC conditions has recently been studied extensively [37]. Guo conducted experiments using an X-series pipeline steel by gravimetric method in a simulated soil solution at various AC densities and frequencies. In his work, the corrosion rate increased with the increase of the AC density, while the AC current involved in the electrode reaction process decreased causing lower corrosion rate of the steel [14].

However, all proposed theories have limitations on the explanation of AC corrosion and have not reached a consensus on the complex corrosion process. Meanwhile, very few studies were dedicated specifically to study the difference in corrosion resistance between various high strength pipeline steels, such as X70 and X80.

The content of C, P and S in X80 steel is lower than in X70 steel, while Mn, Ni, Mo and Nb contents are higher. Elements such as C, P and S have a detrimental effect on the corrosion resistance of metals and alloys, while the metallic elements Mo and Nb help to improve corrosion resistance of pipeline steel [38]. All these factors result in different corrosion resistance of X70 and X80 steel. Study the difference of corrosion behavior between X70 and X80 pipeline steel under AC has important practical significance and theoretical value. Thus, in this paper, the AC corrosion behavior of X70 and X80 pipeline steel in simulated soil solution was compared using gravimetric method, electrochemical test technique and surface analysis method.

## 2. EXPERIMENTAL

### 2.1 Materials and test solution

X70 and X80 pipeline steel (from the First and Second West-East Natural Gas Pipeline Projects, respectively) were selected as experimental materials. The X70 steel microstructure was mainly composed of irregular acicular ferrite, while X80 steel was mainly composed of ferrite, acicular ferrite and sheet bainite. Chemical composition of X70 and X80 is shown in Table 1. The samples were cut into circular pieces  $\Phi 10 \times 2$  mm in size (see Figure 1). Then, the surface of the sample was polished with No. 60-1000 grit followed by washing in deionized water, acetone and absolute ethanol and drying.

**Table 1.** Minor components concentration in X70 and X80 pipeline steel in wt.% (the rest up to 100 wt% is iron).

Steel type	C	P	S	Si	Mn	Cu	Al	Ni	Mo	Nb
X70	0.06	0.008	0.010	0.25	1.66	0.20	0.026	0.18	0.1	0.04
X80	0.04	0.006	0.002	0.22	1.85	0.23	0.04	0.26	0.29	0.1

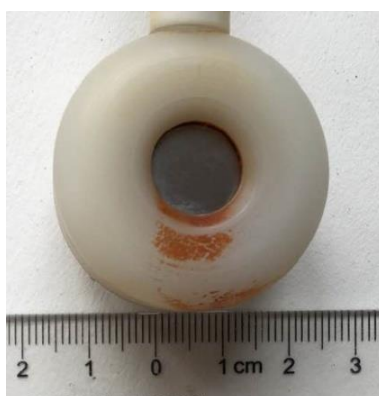


**Figure 1.** Circular experimental sample for the X70 and X80 steel samples

The typical saline soil around Qinghai Salt Lake in China is a Golmud soil with the pH of 8.4. It was selected as the corrosive environment for this study. The ion concentrations of simulated soil solution based on the major physicochemical data of Golmud soil are shown in Table 2. The solutions were prepared using analytical grade NaCl, Na<sub>2</sub>SO<sub>4</sub>, NaHCO<sub>3</sub> and deionized water.

**Table 2.** Components and their concentrations in the simulated soil solution (g/L)

Cl <sup>-</sup>	SO <sub>4</sub> <sup>2-</sup>	HCO <sub>3</sub> <sup>-</sup>	Na <sup>+</sup>
233.30	4.83	0.17	243.12

## 2.2 Electrochemical test

The schematic of the electrochemical test device is shown in Figure 2. Electrochemical measurements were carried out using an electrochemical workstation PARSTAT 2273 (Princeton, NJ, USA). A three-electrode system was used, in which the X70 or X80 pipeline steel were the working electrodes, the saturated calomel electrode was a reference electrode and the platinum plate was the counter electrode. In addition, the SG1005 signal generator, connected to sample and graphite electrodes, was used for AC power. To ensure independence of the two circuits, a 500 μF capacitor was connected to the electric circuits to prevent AC circuits from the interference of DC electrochemical test system. A 15H-inductor was connected to prevent interference with the AC signal. Different AC densities were applied during the immersion and electrochemical tests at a frequency of 50 Hz: 0, 30, 100, 200 and 300 A/m<sup>2</sup>. AC density is equal to the applied AC value divided by the work area.

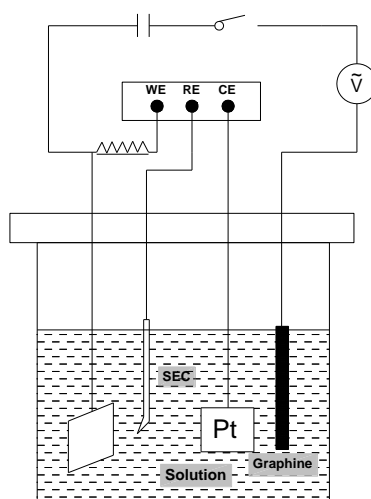


**Figure 2.** Schematic of the electrochemical test setup.

The samples were first placed in the simulated soil solution for 48 h under the AC with a certain density. The work electrodes were held in the test solution for 0.5 h to achieve an electrochemically steady state. Open circuit potential was measured within the next 0.5 h. The polarization curves were recorded at 0.5 mV/s sweeping rate starting from -1000 mV and ending at 700 mV (both relative to the OCP). Final experimental data were fitted using Origin software. The self-corrosion current density  $i_{\text{corr}}$  was compared by the Tafel curve extrapolation method to observe its changing rule.

### 2.3 Corrosion rate and corrosion morphology

Prior to the tests, steel samples were weighed. After the AC corrosion test for 48 h, surface morphology was noted and then, the samples were descaled in a 0.5 g  $\text{Sb}_2\text{O}_3$ +1.5 g  $\text{SnCl}_2 \cdot 2\text{H}_2\text{O}$ +25 ml HCl solution until a complete removal of the corrosion products. The samples were then washed with deionized water, then with acetone and ethanol and weighed again. The corrosion rate was calculated as follow:

$$\Delta W = W_0 - W \quad (1),$$

$$V_{\text{corr}} = 8.76 \times \Delta W / (S \times t \times \rho) \quad (2),$$

where  $\Delta W$  is the average weight-loss of the sample in g,  $W_0$  is the original weight of the sample in g,  $W$  is the sample weight after removing the corrosion products in g,  $S$  is sample exposure area in  $\text{m}^2$ ,  $t$  is the soaking time in h,  $\rho$  is the density of the steel in  $\text{g}/\text{cm}^3$  and  $V_{\text{corr}}$  is the corrosion rate in mm/a.

The microstructure of the corroded surfaces was observed using a high-resolution digital camera and SEM (S-3400, Hitachi, Tokyo, Japan).

## 3. RESULTS AND DISCUSSION

### 3.1 OCP results of X70 and X80 samples

The corrosion potentials of X70 and X80 steel under AC with different densities are shown in Figure 3 (a) - (b). The OCP value shifted negatively after AC was applied to both samples. With the increase of applied AC density from 0 to 30, 100, 200 and 300  $\text{A}/\text{m}^2$ , the open circuit potential of X70 steel in simulated soil solution gradually decreased from -0.792 to -0.848, -0.887, -0.910 and -0.915 V, respectively, while potential of X80 steel gradually decreased from -0.734 to -0.843, -0.878, -0.893 and -0.909 V, respectively. The OCP value for both samples decreased sharply when the AC density increased from 0 to 100  $\text{A}/\text{m}^2$ , however, at AC densities above 100  $\text{A}/\text{m}^2$ , The OCP values showed only a slight negative shift. Typically, the more negative the open circuit potential, the greater the potential difference between the cathode and the anode is, making possibility of metal corrosion higher. Therefore, corrosion resistance of X70 and X80 steel samples decreased with the increase of the applied AC density. This is a good agreement with the previous reports. Jiang [39] observed decreasing corrosion potential of two pipeline samples under the increasing AC current. Li [36]

showed that an increasing AC interference shifted the corrosion potential of X70 steel negatively. Wendt [40] studied that the corrosion resistance of 316 stainless steel was affected by different AC voltages and came to the same conclusions about corrosion potential decrease with the AC voltage increase. In addition, the corrosion potential began to increase with AC only when certain critical values were reached. Our study showed that the OCP values of X70 and X80 steel shifted negatively under the low AC densities (0-100 A/m<sup>2</sup>) quite rapidly, indicating a significant decrease of corrosion resistance. However, the decreasing speed was slow under high AC densities(100 - 300 A/m<sup>2</sup>), indicating that the corrosion resistance of the samples was stable.

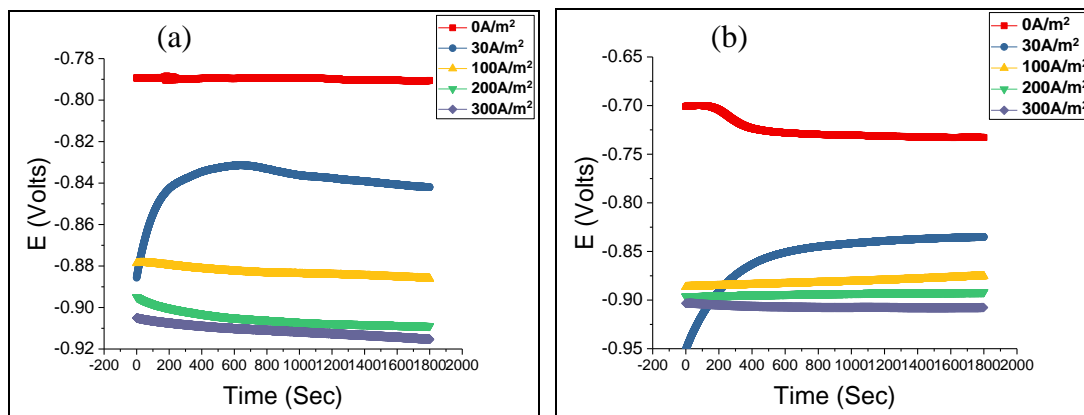


**Figure 3.** OCP vs time curves for (a) X70 and (b) X80 pipeline steel samples at various AC densities.

The OCP values of X70 steel were more negative than that of X80 steel for all AC values (see Figure 3) at the open-circuit potential. During the negative shift of the OCP values, the interface of the double layer formed by the metal/solution becomes unstable due to the AC, which may cause "oscillation" effect [29] and change of the interface voltage. The OCP values of X70 steel was more negative, indicating larger voltage at the electrode/solution interface. Potential difference between cathodic and anodic polarization for X70 steel were larger. Therefore, the corrosion of X70 steel was more serious and X80 steel has better corrosion resistance.

### 3.2 Polarization curves of X70 and X80 samples

Potentiodynamic polarization curves of X70 and X80 steel samples in simulated soil solution at different AC densities are shown in Figure 4. It can be seen from the figure that the AC has a direct impact on both the anode and the cathode curves. In addition, X70 and X80 steel have been in active dissolution state without passivation. Overall, the corrosion potential of X70 and X80 steel negatively shifted with the increase of AC density, which can be described by the following mathematical model [41-43]:

$$E_{corr,AC} = E_{corr} - \left( \frac{b_a}{b_c - 1} \right) \ln \left[ \frac{\sum_{k=1}^{\infty} \frac{1}{(k!)^2} \left( \frac{E_p}{2b_c} \right)^{2k} + 1}{\sum_{k=1}^{\infty} \frac{1}{(k!)^2} \left( \frac{E_p}{2b_a} \right)^{2k} + 1} \right] \quad (3),$$

where  $E_{\text{corr,AC}}$  and  $E_{\text{corr}}$  are the corrosion potentials with and without AC interference,  $b_a$  and  $b_c$  are the Tafel slope of anode and cathode,  $E_p$  is the peak potential of the applied AC and  $k$  is an integer.

The formula (3) shows that the change of corrosion potential caused by AC is a function of the ratio of the Tafel slope of cathode and anode ( $r=b_a/b_c$ ) and  $E_p$ . Since the exposed area of the electrode remains constant during the experiment, the AC density is proportional to the AC peak potential. According to the formula, as  $E_p$  increases, AC density increases as well and the corrosion potential shifts negatively. It can also be seen from Figure 4 that the corrosion potential of X70 and X80 steel moves negatively with the increase of AC density. Therefore, our conclusions are consistent with equation (3): AC interference changes the corrosion potential of X70 and X80 steel, making the corrosion current density positively shift, and the Tafel slope of cathode and anode increase. Although the amplitude of the change is very small, it shows that the corrosion rate of metal is accelerated with the increase of AC density. From a thermodynamic point of view, the metal is more susceptible to be corroded when the corrosion potential becomes negative.

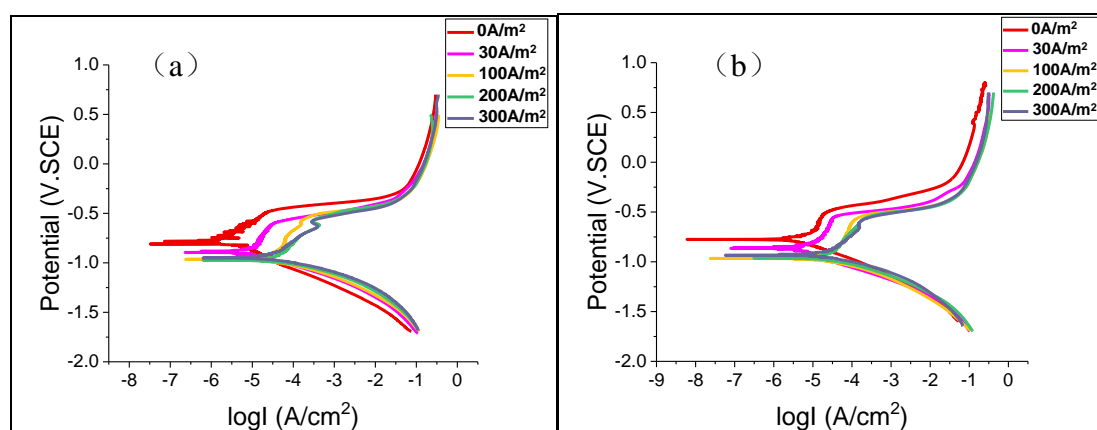


**Figure 4.** Polarization curves of (a) X70 and (b) X80 steel samples at various stray AC densities in simulated soil solution

Kinetic parameters obtained from the fitting of the polarization curves are shown in Table 3 and Table 4. The high value of the self-corrosion potential ( $E_{\text{corr}}$ ) indicates how difficult the corrosion is. The size of the corrosion current density ( $i_{\text{corr}}$ ) indicates the corrosion degree and the speed of the corrosion process. Potentiodynamic polarization curves confirmed results obtained by other methods that the corrosion current density of X70 and X80 steel samples increases, and the corrosion potential shifts negatively at AC density between 0 and 100 A/m<sup>2</sup>. The Tafel slope increases as well and the corrosion degree accelerates during this process. However, the polarization curve and kinetic parameters of X70 and X80 steel also don't change much at high AC density (100-300A/m<sup>2</sup>). The trend of the change depends on the value of  $r$  ( $|b_a/b_c|$ ), which is the ratio of the Tafel slope of the anode and the cathode. The corrosion potential does not shift when  $r = 1$ . The closer  $r$  to 1, the smaller the offset is. When  $r < 1$  or  $r > 1$ , the corrosion potential shifts negatively or positively. According to the kinetic parameters in Tables 3 and 4, the value of  $r$  for X70 and X80 steel becomes closer to 1 with the increase of AC density. Therefore, the shift magnitude of the corrosion potential decreases showing good agreement with the phenomena mentioned above and previous researches.

H. Y. Li [44] concluded that X80 steel has higher corrosion resistance than X70 steel in high concentration solutions. Comparing the anodic polarization curves, no typical passivation zone appeared for both steels. Li [36] investigated the effects of stray alternating current on the corrosion behavior of X70 high strength pipeline steel in a marine soil simulated solution. The results show that with an increase of AC current density, the slopes of anodic and cathodic polarization curves become more vertical, and the corrosion potentials decreased, while the corrosion current density increased slightly. Thermodynamically, the AC interference made the corrosion occurring easily.

**Table 3.** Electrochemical parameters of X70 samples at various AC current density in simulated soil solution

$i(\text{A/m}^2)$	$E_{\text{corr}}(\text{mV})$	$i_{\text{corr}}(\mu\text{A/cm}^2)$	$b_a(\text{mV/dec})$	$b_c(\text{mV/dec})$	$ b_a/b_c $
0	-792.8	8.4	92.6	-263.1	0.35
30	-848.3	29.8	127.9	-347.1	0.37
100	-950.5	121.9	246.1	-376.3	0.65
200	-916.5	113.8	244.7	-395.8	0.62
300	-908.7	59.3	246.9	-403.3	0.61

**Table 4.** Electrochemical parameters of X80 samples at various AC current density in simulated soil solution

$i(\text{A/m}^2)$	$E_{\text{corr}}(\text{mV})$	$i_{\text{corr}}(\mu\text{A/cm}^2)$	$b_a(\text{mV/dec})$	$b_c(\text{mV/dec})$	$ b_a/b_c $
0	-735.0	4.6	70.2	-208.1	0.34
30	-840.9	9.3	115.7	-299.5	0.39
100	-878.7	39.4	163.4	-328.3	0.50
200	-893.7	56.6	186.7	-363.9	0.51
300	-866.2	55.1	230.3	-387.8	0.59

In this paper, the polarization curves of X70 and X80 steel samples are smooth at the low AC density (0-100 A/m<sup>2</sup>), and there is no obvious passivation zone, indicating that X70 and X80 steel samples are always in the activated state(see Figure 4). At the high AC density (100-300 A/m<sup>2</sup>), the anode and cathode reactions of X70 steel are inhibited. The anode curve begins to appear between -600 ~ -700 mV, in which the current density changes little with the increase of the potential. When the potential exceeds this region, the current density greatly increases again, indicating that existence of the pitting potential  $E_{\text{pit}}$  in this region. Above this potential, pitting corrosion can rapidly occur and develop on the surface of X70 steel. At AC density of 300 A/m<sup>2</sup>, the polarization curve of X80 steel

also appears in a similar fashion as X70. Anode reaction and cathode reactions of X80 are inhibited slightly. These observations are consistent with the OCP results of X70 and X80 samples at various AC densities discussed earlier.

Comparison of the corrosion potential and corrosion current density of X70 and X80 steel samples shown in Tables 3 and 4 as well as Figure 4, revealed that the corrosion potential of X70 steel is lower than X80 steel most of the time, while the corrosion current density of X70 steel is always higher than that of X80 steel. According to Faraday's second law, the self-corrosion current density  $i_{\text{corr}}$  ( $\text{A}/\text{m}^2$ ) is proportional to the corrosion rate. Therefore, the corrosion degree of X70 steel is deeper than that of X80 steel, and X80 steel shows better corrosion resistance.

At 200-300  $\text{A}/\text{m}^2$  AC density, corrosion potential and corrosion current density of X80 steel change only slightly, while the corrosion current density of X70 steel decreases and the corrosion potential slightly shifts, indicating that the corrosion process of X70 steel is more obviously inhibited, resulting in slower corrosion.

### 3.3 Experimental results of corrosion rate

The corrosion rates of X70 and X80 steel at different AC densities were also obtained based on the gravimetric method. Corrosion rate trends for X70 and X80 steel samples are similar (see Table 5). Gravimetric results also confirmed that AC interference promotes the corrosion of X70 and X80 steel.

**Table 5.** Gravimetric and corrosion rate test results for X70 and X80 steel samples at various AC current densities in simulated soil solution

$i(\text{A}/\text{m}^2)$	AC current density $i(\text{A}/\text{cm}^2)$	Working area $S(\text{m}^2)$	Soaking time $t(\text{h})$	Mean weight loss $\Delta W(\text{mg})$	Corrosion rate $V_{\text{corr}}(\text{mm}/\text{a})$
X70 pipeline steel	0	$1 \times 10^{-4}$	48h	2.1	0.49
	30	$1 \times 10^{-4}$	48h	6.6	1.54
	100	$1 \times 10^{-4}$	48h	11.0	2.56
	200	$1 \times 10^{-4}$	48h	11.4	2.65
	300	$1 \times 10^{-4}$	48h	11.6	2.70
X80 pipeline steel	0	$1 \times 10^{-4}$	48h	1.8	0.42
	30	$1 \times 10^{-4}$	48h	4.1	0.95
	100	$1 \times 10^{-4}$	48h	4.4	1.02
	200	$1 \times 10^{-4}$	48h	4.9	1.14
	300	$1 \times 10^{-4}$	48h	6.5	1.51

Li [36] concluded that the corrosion the corrosion rate of X70 steel raised with increasing AC current densities, and the corrosion rate is correlated to the anodic current density. Under the interference of AC signal, the anodic process was affected, particularly at the high current density. Guo [14] carried out the laboratory experiments through weight-loss method in a simulated soil solution at various AC densities from 0 to 200  $\text{A}/\text{m}^2$  and frequencies from 10 to 200 Hz, indicating that the corrosion rate increased with the increasing of AC current density. Furthermore, the increase of AC interference frequency caused a lower corrosion rate of pipeline steel. For X60 and X70, when the AC

current density lower than  $150 \text{ A/m}^2$ , the corrosion rate increases as a linear relationship with AC current density approximately. The rising tendency of corrosion rate of X60 and X70 is a little mitigation from  $150 \text{ A/m}^2$  to  $200 \text{ A/m}^2$ .

Comparing the corrosion rate of X70 and X80 steel at each AC density in this paper, we notice that, on one hand, corrosion rate of X70 steel is almost twice as much as that of X80 steel at various AC densities. Corrosion process of X80 steel was only slightly affected by AC interference, confirming yet again, that the corrosion resistance of X80 steel is better. On the other hand, in the absence of cathodic protection, the corrosion rate of X70 steel rapidly and almost linearly increased at the low AC density ( $0\text{-}100\text{A/m}^2$ ), while corrosion rate of X80 steel increased uniformly. Corrosion rate of X70 and X80 steel samples at  $100 \text{ A/m}^2$  AC density was 5.2 and 2.4 times higher, respectively, than without any AC. Thus, the corrosion rate of X70 increased significantly faster than that of X80 at low AC density. However, the change of corrosion rates of X70 steel at high AC density ( $100\text{-}300 \text{ A/m}^2$ ) is very small, indicating slowing-down corrosion. Corrosion rate of X80 steel sample increased more smoothly, and its corrosion resistance was more stable.

### 3.4 Corrosion morphology of X70 and X80 steel

The corrosion appearance on X70 and X80 steel samples at different AC densities is shown in Figures 5 and 6. After the 48 h immersion test, the surface of X70 and X80 samples still had bright metallic luster when there was no AC interference. The samples surface changed significantly under the AC interference showing a lot of corrosion products.

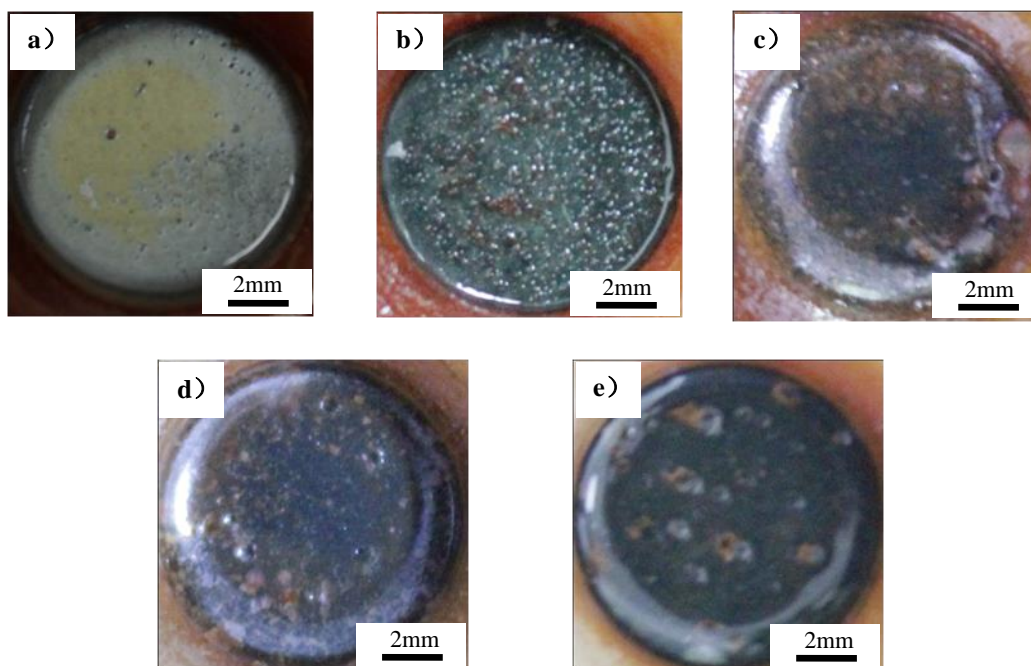


**Figure 5.** Corrosion appearance of the X70 steel samples at (a) 0, (b) 30, (c) 100, (d) 200 and (e) 300  $\text{A/m}^2$  AC densities.

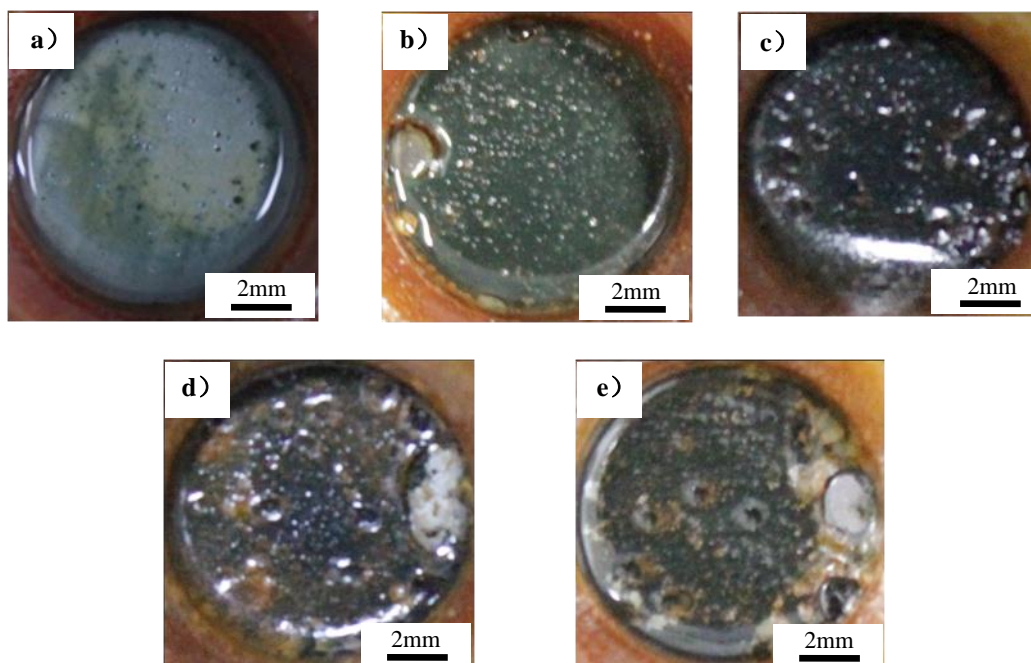


**Figure 6.** Corrosion appearance of the X80 steel samples at (a) 0, (b) 30, (c) 100, (d) 200 and (e) 300 A/m<sup>2</sup> AC densities.

At the same immersion time of 48 h, the accumulated film of corrosion products on both samples became thicker as the AC density increased. At some point corrosion products formed a continuous film, acting as anticorrosion protection for the steel. These observations again agree very well with our previously reported conclusions about corrosion rates at higher AC densities.

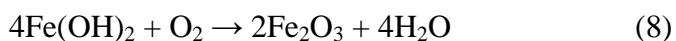
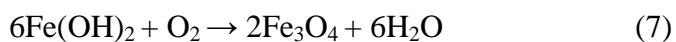
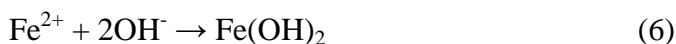
When AC was applied, colorless bubbles were generated on the surface of the samples. Simulated soil solution is an alkaline electrolyte system, in which oxygen reduction occurs on the surface according to the anode and cathode reactions shown in equation (4) and (5), respectively. The oxygen reduction reaction promoted the formation of cathode reaction products and accelerated the corrosion of X70 and X80 steel.



Buchler presented a schematic diagram explaining the mechanism of AC corrosion [45-46]. We modified his proposed mechanism to match observations of our experiments. Since the applied AC signal is sinusoidal, its direction would alternately change, leading to the circulation of anodic and cathodic polarization of the pipeline steel. The inner layer of the macroscopic corrosion product is mainly composed of black products, while the outer layer is mainly composed of brown and reddish products. The inner black material becomes denser with AC density increase and this material is quite difficult to remove with just a cotton swab.

The process of corrosion products accumulation on the surface of pipeline steel under the interference of AC is shown in Equation 6-9. Anodic polarization occurs on the steel surface during the positive half-cycle of the AC disturbance (Equation 4). Then, Fe<sup>2+</sup> and OH<sup>-</sup> combine to form Fe(OH)<sub>2</sub> on the electrode surface (Equation 6). However, the structure of Fe(OH)<sub>2</sub> is relatively loose and it can

transform into  $\text{Fe}_3\text{O}_4$  according to the Equation (7). Cathode polarization occurs on the steel surface during the negative half-cycle of the AC disturbances reducing,  $\text{Fe}_3\text{O}_4$  to  $\text{Fe}(\text{OH})_2$ . As the degree of polarization increases, some  $\text{Fe}(\text{OH})_2$  continues its oxidation to  $\text{Fe}_3\text{O}_4$  and some oxidizes to  $\text{Fe}(\text{OH})_3$  during the next anodic polarization. Therefore, the inner surface of corrosion products of pipeline steel is black  $\text{Fe}_3\text{O}_4$  and the outer corrosion product is reddish  $\text{Fe}(\text{OH})_3$ . As the corrosion process continues,  $\text{Fe}(\text{OH})_3$  is converted into the loose  $\text{Fe}_2\text{O}_3$  and  $\text{FeOOH}$ . However, the dense  $\text{Fe}_3\text{O}_4$  is located in the bottom of the corrosion products, protecting the pipeline steel matrix from further corrosion.



Corrosion products gradually deposit on the surfaces of the samples at low AC density and form a corrosion product film at AC density of  $100 \text{ A/m}^2$ . However, when high AC density is applied to X70 steel, the outermost loose rust layer of X70 steel gradually falls off, while the film of black corrosion products on the inner layer is denser and remains on the substrate protecting it. In contrast, the protective effect on the X80 steel substrate is not very clear due to fewer corrosion products, which form thinner corrosion film.

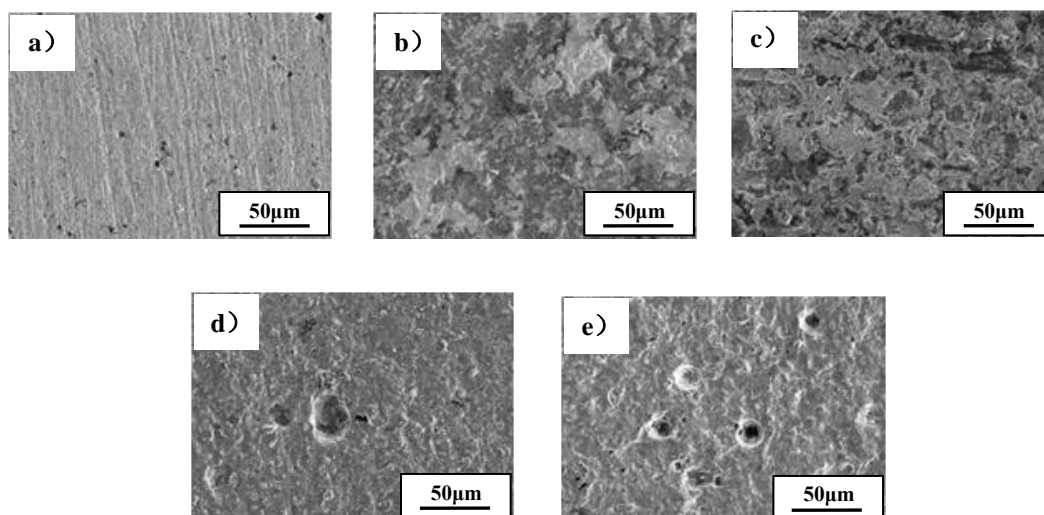


**Figure 7.** SEM images of X70 samples at stray AC densities of (a) 0, (b) 30, (c) 100, (d) 200 and (e)  $300 \text{ A/m}^2$

After removing the corrosion products, the microscopic corrosion morphology of the samples was observed by a scanning electron microscope (see Figures 7 and 8). At low or zero AC density, the surfaces of X70 and X80 steel were smoother and their surface morphology after the corrosion looked uniform. At AC density above  $100 \text{ A/m}^2$ , the surface of X70 steel became rough and with more corrosion pits, which gradually became deeper. Localized corrosion occurred on the surface of

samples, showing obvious pitting morphology. As we mentioned above, the corrosion film acts as a protective barrier, however, such corrosion product film would be destroyed at the thinner areas, allowing pitting corrosion to progress at high AC density.

On the contrary, X80 steel shows uniform corrosion at AC density of 0-200 A/m<sup>2</sup>, and the samples surface looks flat. When the AC density increases to 300 A/m<sup>2</sup>, slight pitting corrosion appeared on the X80 steel surface, indicating lesser corrosion degree of the X80 steel comparing to X70 steel, thus, fewer corrosion products and thinner corrosion film. Therefore, the corrosion resistance of X80 steel is more stable.

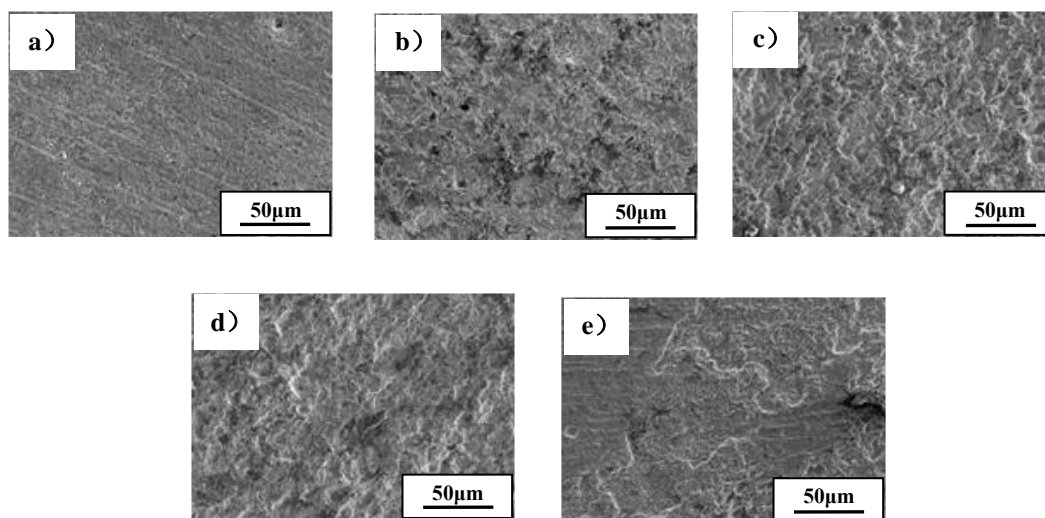


**Figure 8.** SEM images of X80 samples at stray AC densities of (a) 0, (b) 30, (c) 100, (d) 200, and (e) 300 A/m<sup>2</sup>

The difference in corrosion behavior is attributed to the differences in the chemical composition of the material [36]. Metal corrosion often occurs along the boundaries of the alloy grains and their adjacent areas, while the corrosion of the grains themselves is minor. The accumulation of C, P, S and other inclusions in the grain boundary leads to the lower potential comparing to that one of the grain. In thermodynamics, the lower the equilibrium potential, the higher the activity of the metal is. This explains why the anode dissolves first during the corrosion process. Therefore, elements such as C, P and S affect corrosion behavior of the pipeline steel [37]. Concentration of these elements in X80 steel is lower than that in X70 steel (see Table 1). In addition, X80 steel has higher content of Mn, Ni, Mo and Nb than X70 steel. Since C, P, S elements are detrimental and Mn, Ni, Mo and Nb elements are beneficial to corrosion resistance of metals [38], X80 steel shows better corrosion resistance than X70 steel under AC interference [14].

#### 4. CONCLUSIONS

(1) As the AC density increased, the X70 and X80 steel showed similar electrochemical characteristics during their corrosion in simulated soil solution. The corrosion potentials shifted negatively. The polarization curves contained only active dissolution zones and no passivation zone,

indicating that the corrosion possibility of X70 and X80 steel under AC interference significantly increased.

(2) At the low AC density between 0 and 100 A/m<sup>2</sup>, the corrosion rate of X70 steel rapidly increased with the increase of the current density. At AC density of 100 A/m<sup>2</sup>, the corrosion rate of X70 steel was about 5.2 times higher than without AC interference. The corrosion rate did not change noticeably at the high current density (100-300A/m<sup>2</sup>), indicating that the corrosion behavior of X70 steel was relatively stable at this range. Under the action of AC from 0 to 300 A/m<sup>2</sup>, the corrosion rate of X80 steel increased steadily with the current density increase. The corrosion rate of X80 steel at AC density of 100 A/m<sup>2</sup> was about 2.4 times higher than that without the AC interference and about 0.7 times than that at AC density of 300 A/m<sup>2</sup>. Under the interference of AC at the same density, the corrosion rate of X70 steel was about twice than that of X80 steel. Thus, the corrosion resistance of X80 steel is much better than X70 steel, and its corrosion resistance is more stable.

(3) At the low AC density (0 A/m<sup>2</sup> - 100 A/m<sup>2</sup>), the surface of X70 sample was smooth and uniform. However, due to the localized corrosion, the sample surface becomes rough with numerous corrosion pits at high AC density (100-300 A/m<sup>2</sup>). The thinner areas of corrosion products are destroyed to form pits at high AC density. In the current density range of 0–200 A/m<sup>2</sup>, the corrosion morphology of X80 steel is uniform, and the sample surface is relatively flat. When the current density is increased to 300 A/m<sup>2</sup>, some pitting corrosion is observed on the surface of X80 steel with fewer corrosion products. Thus, X80 steel has better corrosion resistance under AC interference than X70 steel.

#### ACKNOWLEDGEMENTS

This work was supported by National Natural Science Foundation of China (No. 51471011) and “Rixin Scientist” of Beijing University of Technology.

#### References

1. A. J. Brito, A. T. D. Almeida, *Reliab. Eng. Syst. Safe.*, 94 (2009) 187.
2. M. Zhu, C. Du, X. Li and H. Li, *Corros Sci.*, 87 (2014) 224.
3. D. Tang, M. Lu and Y Du, *Corros.*, 71 (2015) 795.
4. H. R. Hanson and J. R. Smart, *Corros.*, (2004).
5. S. Goidanich, L. Lazzari, and M. Ormellese, Influence of AC on corrosion kinetics for carbon steel, zinc and copper, NACE Corrosion/2005, Houston TX, USA, 2005, Paper No.05189.
6. R. G. Wakelin and C. G. Sheldon, Investigation and mitigation of AC corrosion on a 300 mm diameter natural gas pipeline, NACE Corrosion/2004, New Orleans, La, 2004, Paper No. 042059.
7. Y. Hosokawa, Overcoming the new threat to pipeline integrity - AC corrosion assessment and its mitigation, 2008.
8. J. Zhao, F Xie and K Gong, *Surf. Technol.*, 46 (2017) 108.
9. G. X. Zhong, Q. Shi and Q. K. Zhao, *Surf. Technol.*, 45 (2016) 106.
10. K. Huang, J. L. Wu and K. Quan, *Surf. Technol.*, 47 (2018) 116.
11. Z. S. Li, Z. Y. Liu and C. W. Du, *Surf. Technol.*, 45 (2016) 1.
12. X. Li, Q. J. Zhu and N. Zhu, *Surf. Technol.*, 46 (2017) 206.
13. S. Bordbar, M. Alizadeh and S.H. Hashemi, *Mater. Des.*, 45 (2013) 597.
14. Y. GUO, T. Meng, D. Wang, H. Tan and R. He, *Eng Fail Anal.*, 78 (2017) 87.
15. Z. G. Chen, C. K. Qin and J. X. Tang, *J. Nat. Gas Sci. Eng.*, 15 (2013) 76.

16. S. R. Allahkaram, M. Isakhani-Zakaria and M. Derakhshani, *J. Nat. Gas Sci. Eng.*, 26 (2015) 453.
17. A. O. S. Solgaard, M. Carsana and M. R. Geiker, *Corros Sci.*, 74 (2013) 1.
18. B. McCollum and G. H. Ahlborn, *J. Franklin. I.*, 182 (1916) 108.
19. H. E. Haring, *J. Electrochem. Soc.*, 99 (1952) 30.
20. F. E. Kulman, *Corros.*, 17 (1961) 34.
21. J. F. Williams, *Mater. Prot.*, 5 (1967), 52.
22. W. H. Brucker, The effects of 60 cycle alternating current on the corrosion of steels and other metals buried in soil, Illinois: Engineering Experiment Station Bulletin 470, University of Illinois, Urbana, 1964.
23. D. T. Chin and T. W. Fu, *Corros.*, 35 (1979) 514.
24. A. W. Hamlint, *Mater. Perform.*, 57 (1986) 57.
25. S. B. Lalvani and X. Lin, *Corros Sci.*, 38 (1996) 1709.
26. R. W. Bosch and W. F. Bogaerts, *Corros Sci.*, 40 (1998) 323.
27. L. Nielsen, *Corros.*, (2005).
28. F. E. KULMAN, *Corros.*, 17 (2005) 34.
29. S. Goidanich, L. Lazzari and M. Ormellese, *Corros Sci.*, 52 (2010) 916.
30. D. A. Jones, *Corros.*, 34 (1978) 428.
31. L. V. Nielsen and F. Galsgaard, Sensor technology for on-line monitoring of AC-induced corrosion along pipelines, NACE Corrosion/2005, Houston TX, USA, 2005.
32. S. Goidanich, L. Lazzari and Ormellese M, *Corros Sci.*, 52 (2010) 916.
33. A. Q. Fu and Y. F. Cheng, *Corros Sci.*, 52 (2010) 612.
34. L. Y. Xu, X Su and Z. X. Yin, *Corros Sci.*, 61 (2012) 215.
35. M. Ormellese, L. Lazzari and A. Brenna, Effects of AC-interference On Passive Metals Corrosion, NACE Corrosion/2011, Houston TX, USA, 2011, Paper No.11342.
36. Y. C. Li, C. Xu and R. H. Zhang, Q. Liu, X. H. Wang and Y. C. Chen, *Int. J. Electrochem. Sci.* 12 (2017) 1829.
37. P. Liang, X. G. Li, C. W. Du and C. Xu, *Mater. Des.*, 30 (2009) 1712.
38. F. Mohammadi, F.F. Eliyan, A. Alfantazi, *Corros Sci.*, 63 (2012) 323.
39. Z. T. Jiang, Y. X. Du, M. X. Lu, Y. N. Zhang, D. Z. Tang, L. Dong, *Corros Sci.*, 81 (2014) 1.
40. J. L. Wendt and D. T. Chin, *Corros Sci.*, 25 (1985) 889.
41. P. J. Gellings, *Electrochimica Acta.*, 7 (1962) 19.
42. H. Xiao and S. B. Lalvani, *J. Electrochem. Soc.*, 155 (2008) C69.
43. R. Zhang, P. R. Vauravanathan and S. B. Lalvani, *Corros Sci.*, 50 (2008) 1664.
44. H. Y. Li, K. Wei and J. D. Hu, *Trans. Mater. Heat. Treat.*, 32 (2011) 151.
45. M. Büchler and H.-G. Schöneich, *Corros.*, 65 (2012) 578.
46. M. Zhu, C. Du and X. Li, *Electrochimica Acta.*, 117 (2014) 351.